



Non-Linear Mechanical Behavior of Plasma Sprayed Alumina Under Mechanical and Thermal Loading

Radek Musalek, Jiri Matejcek, Monika Vilemova, and Ondrej Kovarik

(Submitted April 24, 2009; in revised form June 30, 2009)

Mechanical response of plasma sprayed ceramic coatings to mechanical and thermal loading of various extents was studied. Coated samples were subjected to four-point bending (4PB), with coatings loaded in tension and compression, respectively. Thermal loading was provided by heating the samples, while stresses were generated by thermal mismatch between the coatings and substrates. In both cases, cyclic loading was applied. Non-linear behavior and significant hysteresis were observed, indicating inelastic phenomena taking place. The tests were complemented by structural observations in SEM and indentation tests. Relevant structural features and possible mechanisms underlying this behavior are discussed.

Keywords APS coatings, fatigue and fracture, hardness and (visco-) elastic properties, influence of spray parameters, stiffness, thermal cycling

1. Introduction

Plasma sprayed coatings have a typical inhomogeneous microstructure, consisting of flattened particles—splats—and pores, cracks and weakly bonded interfaces. As a consequence, their mechanical properties are largely different from bulk materials. Characteristic features include relatively low Young's moduli, mechanical anisotropy, non-linear stress-strain relationship, including elastic and/or inelastic phenomena, and different behavior in tension and compression (Ref 1). Various deformation mechanisms, different from bulk materials, may operate in

This article is an invited paper selected from presentations at the 2009 International Thermal Spray Conference and has been expanded from the original presentation. It is simultaneously published in *Expanding Thermal Spray Performance to New Markets and Applications: Proceedings of the 2009 International Thermal Spray Conference*, Las Vegas, Nevada, USA, May 4-7, 2009, Basil R. Marple, Margaret M. Hyland, Yuk-Chiu Lau, Chang-Jiu Li, Rogerio S. Lima, and Ghislain Montavon, Ed., ASM International, Materials Park, OH, 2009.

Radek Musalek and **Monika Vilemova**, Department of Materials Engineering, Institute of Plasma Physics, Za Slovankou 3, 182 21 Praha 8, Czech Republic; and Department of Materials, Faculty of Nuclear Sciences and Physical Engineering, Czech Technical University in Prague, Trojanova 13, 120 00 Praha 2, Czech Republic; **Jiri Matejcek**, Department of Materials Engineering, Institute of Plasma Physics, Za Slovankou 3, 182 21 Praha 8, Czech Republic; and **Ondrej Kovarik**, Department of Materials, Faculty of Nuclear Sciences and Physical Engineering, Czech Technical University in Prague, Trojanova 13, 120 00 Praha 2, Czech Republic. Contact e-mail: musalek@ipp.cas.cz.

plasma sprayed coatings and are responsible for the above-mentioned behavior. These may include crack opening and closing, formation of new cracks, mutual sliding or torsion of the interfaces and generally inhomogeneous deformation. On the other hand, the coating structure and consequently its properties can be significantly influenced by processing conditions (Ref 2).

The objective of this study was to explore the mechanical response of plasma sprayed alumina coatings to various forms of loading, relate it to the coating structure and selected processing parameters. Alumina was selected as a representative material because of its widespread use and applicability in thermal and wear protection (Ref 3) and, as a typical ceramic material, because of expected sensitivity to the presence, distribution and formation of cracks.

2. Experimental Procedure

White alumina powder of 30-80 μm size (AB230, Carborundum Electric, Benatky n. J., Czech Republic) was sprayed by water-stabilized plasma system WSP[®] (Institute of Plasma Physics, Praha, Czech Republic) at three different settings (Table 1), which were expected to result in coatings with different densities and stiffnesses. The feed rate was 10 kg/h in all cases and the deposition temperature was kept below 280 °C. For four-point bending (4PB) test the substrates were $3.18 \times 25 \times 100$ mm Ti6Al4V and $2.59 \times 25 \times 100$ aluminum (A199.5). The substrates were annealed prior to deposition to eliminate stresses unrelated to spraying. Ti6Al4V was chosen for its relatively low modulus and high elastic limit that permits testing of the coatings up to relatively large strains, while aluminum is easily deformable. Coating thicknesses were around 1 mm, in order to have a sufficient coating contribution to the total stiffness in 4PB. For thermal cycling, 0.2-mm-thick coatings were sprayed on

Table 1 Spraying parameters

| Notation | Spray distance, mm | Feed distance, mm | T , °C | v , m/s | Resulting α -phase content, % |
|----------|--------------------|-------------------|----------|-----------|--------------------------------------|
| 40-350 | 40 | 350 | 2171 | 97 | 8 |
| 60-425 | 60 | 425 | 2105 | 83 | 6 |
| 80-500 | 80 | 500 | 2084 | 77 | 20 |

2.5 × 25 × 230 mm aluminum substrates. In this case, reduced coating thickness had to be used, otherwise the thermal mismatch stress would produce plastic deformation in the substrates even at moderate temperatures.

During the spraying session, particle temperatures and velocities were monitored by a DPV-2000 diagnostic system (Tecnar, St. Bruno, Canada), in a matrix of 5 × 5 points 9 mm apart, perpendicular to the spray plume at spraying distance.

Ratio of the α and γ phases in the coatings was determined by x-ray diffractometer Siemens D500 (Siemens, Karlsruhe, Germany).

Specimens for structural observation and indentation test were prepared using standard metallographic procedure (grinding and polishing). Indentation modulus was determined with indentation instrument NanoTest (Micro Materials Limited, Wrexham, UK) with WC-Co spherical indenter ($r=0.79$ mm) and maximum load 5 N. The indentation modulus was determined from the measured load-displacement curve using Oliver-Pharr method. Bonded-interface technique (Ref 4) was used for one of the 80-500 coatings to observe changes in the microstructure after permanent deformation. Spherical indent across the bonded interface was created using EMCO-TEST M4C (Kuchl, Austria). Cross sections were observed with JEOL 5510 LV (Jeol, Tokyo, Japan) scanning electron microscope.

4PB (Fig. 1) was performed on universal testing machine Inspekt 100 (Hegewald-Peschke, Nossen, Germany) with a fully articulating fixture having 85 mm outer span and 47 mm inner span. Specimen deflection was measured with adapted strain gauge extensometer Instron 2620-603 (Instron, Norwood, USA). Coatings on substrates were loaded in tension or compression by choosing their orientation in the fixture. Different specimens were used for loading in compression and tension. Three loading modes were used consequently for each specimen (Fig. 2):

- loading up to stepwise increasing loads, with full unloading (mode I),
- loading up to the maximum load, with full unloading (mode II), and
- loading up to stepwise increasing loads, with partial unloading (mode III).

This allowed us to observe the coating behavior at different load levels and hysteresis of the stress-strain curves. Coating secant modulus was separated from the total stiffness (Ref 5). Bare substrates were tested to assess their elastic limits. The maximum load applied was then selected accordingly.

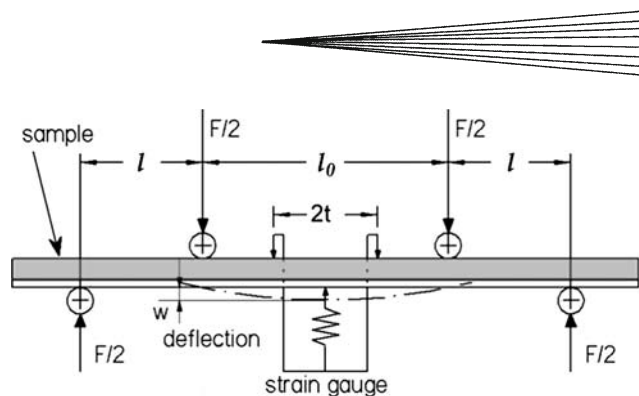


Fig. 1 Experiment setup for 4PB test (Ref 8). $l_0=47$ mm, $l=19$ mm, $t=16$ mm

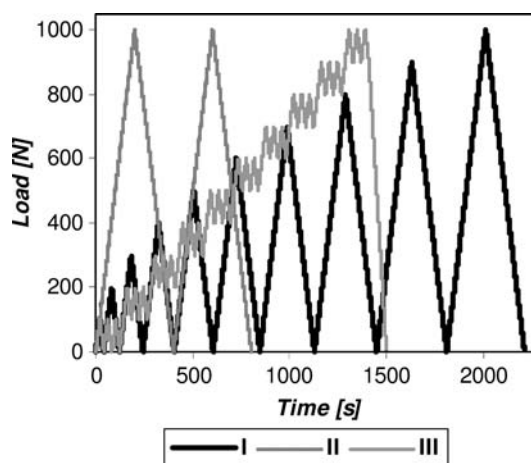


Fig. 2 Loading modes for 4PB test

Thermal loading was applied in a house-made fixture, consisting of a heating element ensuring uniform heating of the specimen and a laser triangulation distance sensor, traversing along the specimen in a controlled fashion, permitting to determine the curvature at selected temperature intervals (Ref 6). With the dimensions, coefficients of thermal expansion of both materials and Young's modulus of the substrate known, Young's modulus of the coating as a function of temperature or strain was determined as described in Ref 7. For each specimen, four cycles up to 200 °C with 0.1 °C/s rate were performed.

3. Results

Characteristic microstructures of the deposits in half-thickness of the coating can be seen in Fig. 3. Slight differences in splats morphology correspond to differences in deposition conditions.

Values of indentation modulus determined from instrumented indentation from the surface (cross-sectional modulus) and cross-section side (in-plane modulus) are plotted in Fig. 4. Plot shows significant scatter of the data due to porous structure of the coating. Significant difference in stiffness of the material was observed for loading from the surface and cross-section side. This behavior is

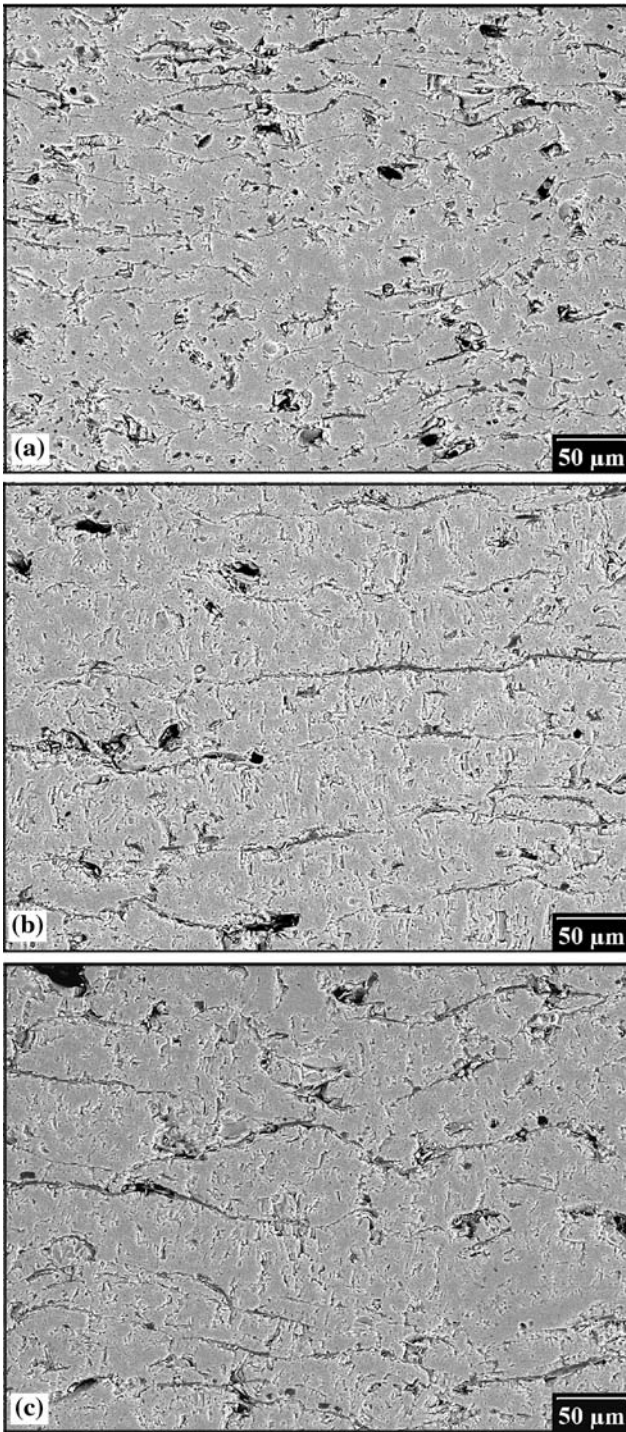


Fig. 3 Microstructures of sprayed coatings. SEM image—backscattered electrons (COMPO). (a) 40-350, (b) 60-425, and (c) 80-500

caused by the lamellar structure of the material with preferential orientation. For different spraying conditions, no significant difference in indentation behavior was observed.

Permanent changes in microstructure during indentation were observed with bonded-interface technique. Comparing

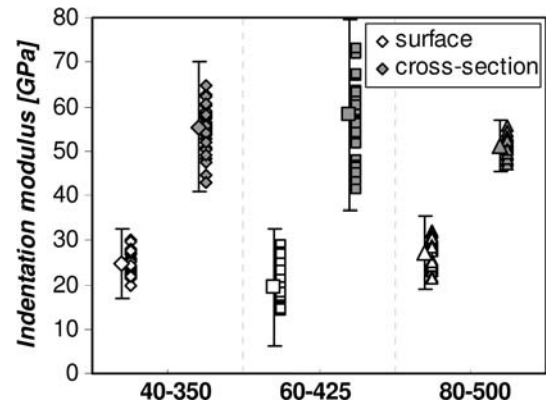


Fig. 4 Indentation moduli determined from instrumented indentation

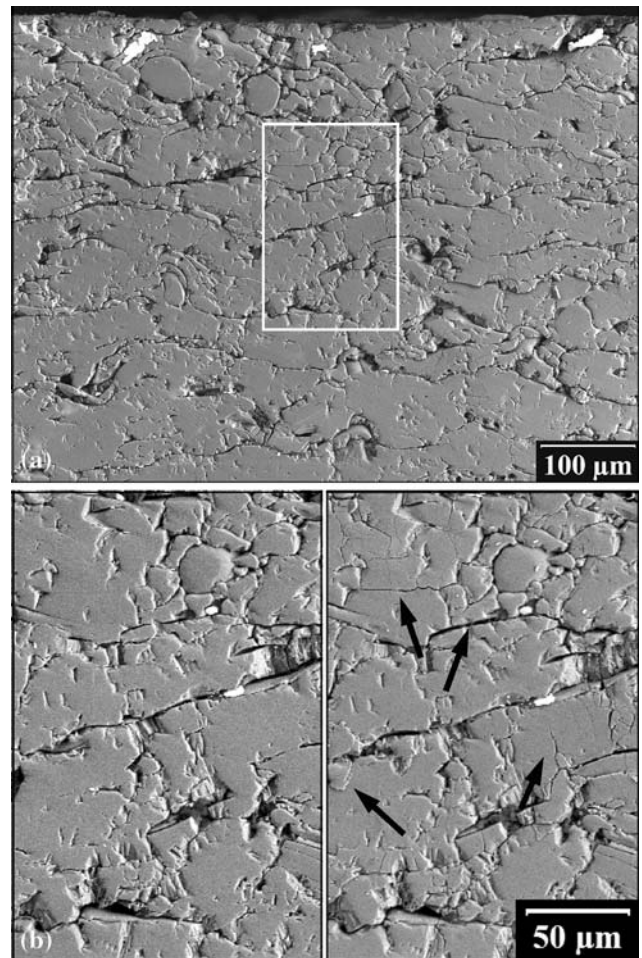


Fig. 5 Coating 80-500 cross-section under indent ($r=1.25$ mm, load 613.13 N). SEM image—backscattered electrons mode (COMPO). (a) Coating microstructure under indent (after indentation); (b) detail of highlighted area before (left) and after (right) the indentation

images of the same spot before and after loading (Fig. 5) shows significant cracking, debonding, and mutual sliding of the splats along with cracks closing which led to the coating

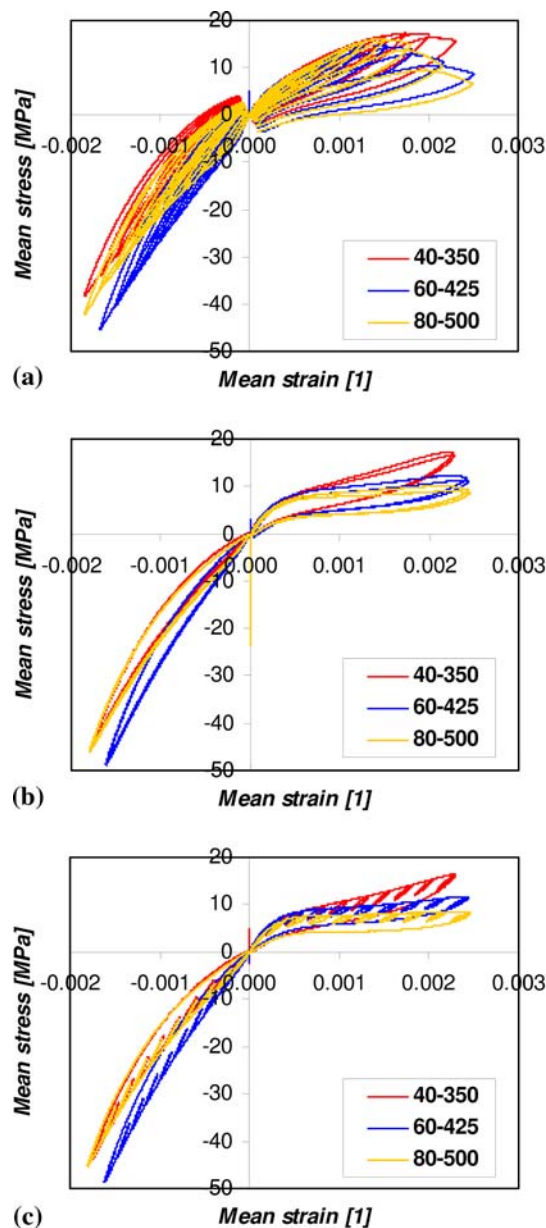


Fig. 6 Mean stress vs. mean strain in the coating evaluated from 4PB test. Loading modes I, II and III applied consecutively. Ti6Al4V substrate. (a) Loading mode I, (b) loading mode II, and (c) loading mode III

compaction. Such changes in microstructure were observed up to 800 μm depth under the indent.

Load-deflection curves obtained from 4PB test were transformed to plots showing evolution of mean stress-mean strain curves (Fig. 6) and dependence of coating secant modulus on mean strain (Fig. 7).

From the character of the loading curves the following statements can be made for tested alumina coatings:

- Qualitative difference in coating behavior in compression and tension can be observed. Stiffness of the coating increased with increasing compressive strain and decreased with increasing tensile strain.

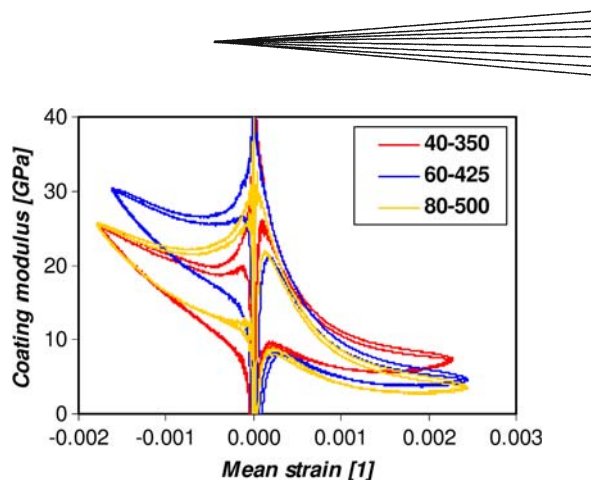


Fig. 7 Coating secant modulus vs. mean strain evaluated for curves from Fig. 6(b) (loading mode II)

- No qualitative differences in mechanical behavior were observed for specimens deposited at different conditions, although slight differences in modulus values were registered.
- Coating stiffness evaluated in terms of effective secant coating modulus dropped in the achieved strain range from ca. 25-30 GPa for mean strain -0.16% (compression) to 4-7 GPa for mean strain 0.22% (tension).
- The first loading curve differs from the subsequent curves to the same loading level, which signifies irreversible changes in the coating microstructure (namely cracks evolution, splat debonding, mutual splat sliding, etc.) even from initial levels of applied strain. Local coating changes lead to the release of the residual stresses in the coating and therefore some residual permanent bending was observed. If the load level was further increased, loading path differed again from the subsequent stabilized curves.
- The determined stress-strain curves exhibit significant non-linearity in the whole range of tested strains.
- Hysteresis indicating energy dissipation in the material due to internal friction was noted for all loading modes. It also indicates that some changes in the coating may be reversible (e.g. pores closing or mutual splat sliding).
- From the stress-strain curves maximum (Fig. 6a) one can estimate the tensile strain level causing large-scale cracking of the coating and loss of coating stiffness (ca. 0.15% corresponding to effective mean stress approx. 15 MPa).

The maximum loading (1000 N) admissible by the 4PB fixture was insufficient to achieve macroscopic failure of the coating on Ti6Al4V substrates. Therefore, previously tested specimens were cut longitudinally in two halves to reduce their stiffness (thereby doubling the maximum strain achieved) and tested again in mode I (Fig. 8). Note changed character of the stress-strain curve due to the previous loading history. In tension, further decrease in coating stiffness continued until total loss of stiffness of the coating due to delamination at

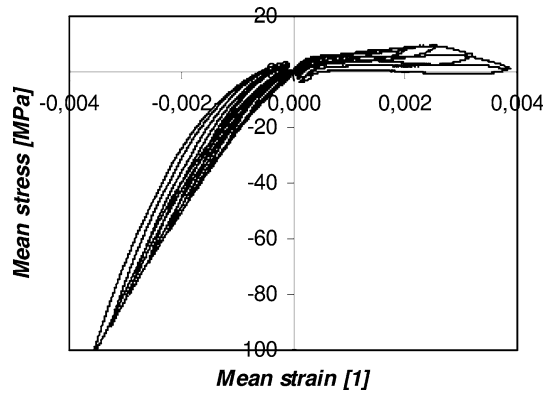


Fig. 8 Mean stress vs. mean strain in the coating evaluated from 4PB test of half specimen. Coating 40-350 on Ti6Al4V substrate

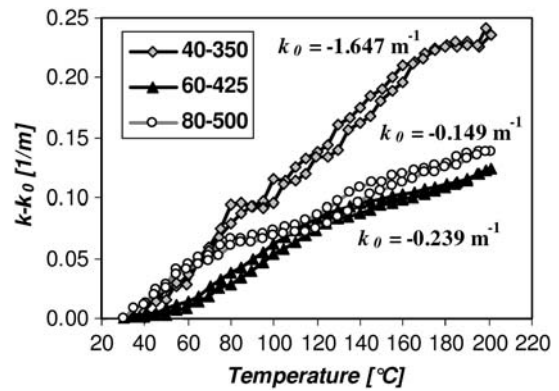


Fig. 10 Specimen curvature evolution during the fourth thermal cycle. k_0 illustrates initial specimen curvature at room temperature. Al99.5 substrate

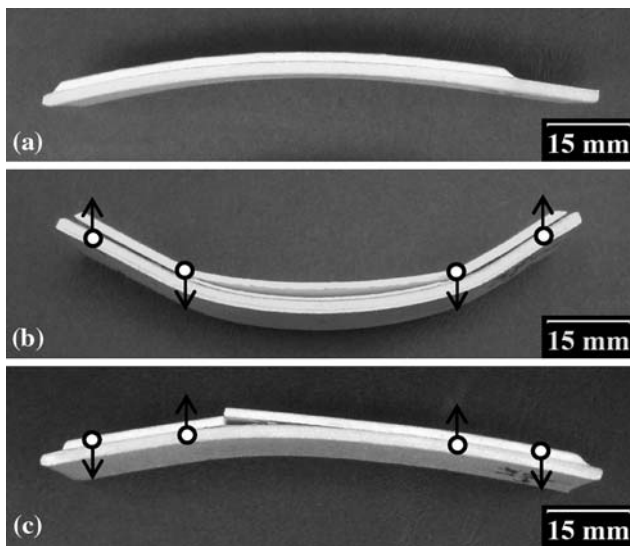


Fig. 9 4PB test of specimen coating 60-425 on Al99.5 substrate. (a) Specimen prior to the loading; (b) compression loading—failure strain $\epsilon_c = -1.36\%$; and (c) tensile loading—failure strain $\epsilon_c = 0.26\%$

the coating-substrate interface. At the same time, major cracking perpendicular to coating surface was observed for each coating (40-350, 60-425, 80-500) at tensile mean strain (0.40, 0.32 and 0.32%, respectively). In compression, further increase in coating stiffness was observed but large-scale failure was not reached until maximum applicable load (1000 N).

Specimens with 60-425 coating on 99.5Al substrate were loaded using 4PB test both in tension and compression until failure of the coating. Residual stresses in the coating resulted in noticeable curvature of the specimens after spraying (Fig. 9a). Due to a low yield stress and therefore extensive plastic deformation of the substrate, only mean strain estimate could be evaluated from the load-curvature record. Significant difference in coating failure in compression and tension was observed (Fig. 9b and c). In compression, permanent change of the coating

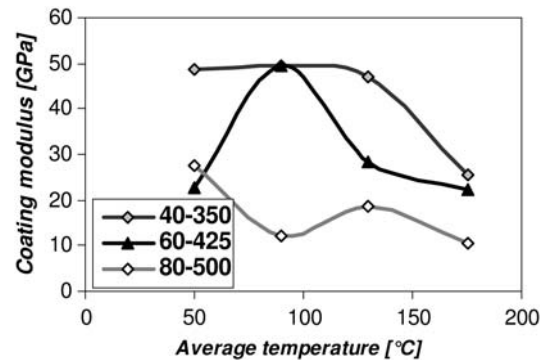


Fig. 11 Coating modulus evaluated from thermal cycling. Average for heating and cooling curve

curvature was observed between inner supports and coating failed at relatively high strain (-1.36%) due to the cracking under the inner supports and loss of the coating cohesion. In tension, coating failed at noticeably lower strain (0.26%) which was comparable to the previous experiment with Ti6Al4V substrate. Failure of the coating was due to the delamination of the coating and major cracking in the plane perpendicular to the coating-substrate interface.

Figure 10 shows the curvature change $k - k_0$ (k_0 denotes curvature at room temperature) versus temperature for thermal cycle of the coating specimens on 99.5Al substrate. The other cycles followed practically the same path. The graph shows a noticeable hysteresis and an overall decrease in slope toward higher temperatures. This indicates decreasing coating modulus. The coatings were initially under compression, and moved toward tension upon heating.

Figure 11 shows Young's modulus of the coatings evaluated from the thermal cycles in four temperature intervals. Apart from local variations, an overall trend of decreasing modulus with increasing temperature (toward tension) can be seen. If the modulus was plotted against absolute strain, the starting points would be different for

each coating (40-350, 60-425, 80-500) due to different residual strain (-0.22 , -0.03 , and -0.02% , respectively), but the trends would be the same.

4. Discussion

Since the feedstock contained 100% α -phase, its higher content in the 80-500 coatings (with the lowest particle temperature and velocity) (Table 1) likely originates from the incompletely molten feedstock particles. On the other hand, in the case of 40-350 coating, higher particle temperature and velocity combined with specimen heating caused by short spray distance could result in more sintered coating with stronger bonding between splats.

Values of the indentation modulus from the instrumented indentation can be slightly influenced by the fact that cross-section samples were embedded in epoxy resin while samples for surface indentation were free-standing.

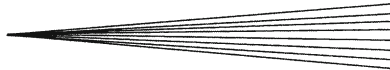
Conditions under indent during the bonded-interface test are different from conditions in as-sprayed coating. After fastening the sample interfaces together in a special sample holder, the resulting gap between the interfaces was ca. 10 μm . The gap was filled with thermoplastic resin helping to stick samples together. Therefore, mutual sliding of the splats was not fully constrained across the interface. On the other hand, splats in porous coatings are also not thoroughly constrained, unlike in the bulk material. Secondly, only permanent deformation of the structure under the indent can be studied using this technique. Reversible elastic deformation could not be observed.

4PB test evaluation used in this paper can provide estimate of stress-strain curve for the coating. Its maximum in tension indicates loading level, where significant changes in the coating can occur. In the case of coating on the deformable substrate, further increase of load causes gradual evolution of coating failure (cracks evolution, splat debonding, etc.) but the coating could be still operational. On the other hand, sudden fracture would occur in the case of free-standing coating.

High values of coating modulus determined from 4PB test near zero applied strain could be caused by combination of high initial stiffness due to the initial static friction or measurement error at extremely low loads.

In the whole paper, effective mean stress and mean strain in the central plane of the coating are considered (Ref 5). Local stress and strain values near the stress concentrators, such as cracks, loose splats, etc., can be significantly higher. Stress and strain levels at the free surface of the coating during bending can also be slightly higher than their mean values due to the higher distance from neutral axis of the specimen.

During thermal loading, specimens showed non-linearity and hysteresis, but the extent of these effects was smaller than in the case of 4PB loading because the magnitude of achieved strain was ca. 1 order lower, which was insufficient for effective changes in the coating microstructure.



In this paper, stress and strain originating only from external loading are considered. Due to the stiffness of the Ti6Al4V substrate and therefore small specimen curvature, residual stresses could not be reliably evaluated from it. Using other technique will be considered in future work.

5. Conclusions

Deformation behavior of sprayed alumina was studied using mechanical (4PB and indentation) and thermal cycling. Tested alumina coatings exhibited non-linear, inelastic, inhomogeneous, anisotropic, and irreversible behavior.

Deformation of the coating was “pseudoplastic”, since ceramic material is not expected to exhibit plastic deformation under the testing conditions. Mechanisms of permanent coating deformation were identified as splat debonding and mutual sliding, compaction of the material, cracking of the splats and pores and cracks interlinking. In the case of the metallic coatings, plastic deformation of the splats is expected, which could delay premature failure of the coating.

Although modulus values determined with different methods can differ (due to, e.g., different load mode and direction, level of deformation), overall trends are the same. Gradual decrease in coating stiffness was observed during tensile loading, which finally led to the failure of the coating. In compression, significantly higher capability to withstand extensive deformation was observed. Such behavior of thermally sprayed ceramics is a consequence of splat-like structure and can be advantageous for many engineering applications compared to bulk ceramics. It also corresponds to the idea of closing of pores and cracks during compression and cracks formation and opening during tension. Kroupa's model of non-linear behavior of thermally sprayed ceramics (Ref 1) therefore seems to be appropriate for alumina coatings tested.

Higher coating modulus means its higher stiffness, better bonding of the splats etc. But it also means higher stress level in the coating, because coating strain is usually driven by substrate strain. Therefore, coating failure strain should also be considered for coating application to provide coating operability and avoid its failure. It should always be higher than permissible strain level of the substrate. For example, let us assume that critical strain for steel substrate is the engineering 0.2% offset strain. Under such assumption, the tested thermally sprayed coatings should be operational in both compression and tension.

As it is obvious from the presented results, significant changes in mechanical properties of the plasma sprayed ceramic coatings can be expected even at low levels of loading. Therefore, modulus value of sprayed ceramic coatings determined using 4PB test should always be linked with the achieved strain.

Results presented in this paper show good agreement with previously published data for other sprayed ceramics (Ref 5, 8, 9).

Acknowledgments

Financial support from Czech Ministry of Education, Youth and Sports through grant no. ME901 and Czech Science Foundation grant No. 106/08/1240, as well as the help of Brian Choi and Lorena Bejarano (CTSR at Stony Brook University, USA) are gratefully acknowledged.

References

1. F. Kroupa, Nonlinear Behavior in Compression and Tension of Thermally Sprayed Ceramic Coatings, *J. Therm. Spray Technol.*, 2007, **10**(1), p 84-95
2. S. Sampath, X. Jiang, A. Kulkarni, J. Matejicek, D.L. Gilmore, and R.A. Neiser, Development of Process Maps for Plasma Spray: Case Study for Molybdenum, *Mater. Sci. Eng. A*, 2003, **348**(1-2), p 54-66
3. P. Chraska, J. Dubsy, K. Neufuss, and J. Pisacka, Alumina-Base Plasma-Sprayed Materials Part I: Phase Stability of Alumina and Alumina-Chromia, *J. Therm. Spray Technol.*, 1997, **6**(3), p 320-326
4. L. Prchlik, J. Pisacka, and S. Sampath, Deformation and Strain Distribution in Plasma Sprayed Nickel-Aluminum Coating Loaded by a Spherical Indenter, *Mater. Sci. Eng. A*, 2003, **360**(1-2), p 264-274
5. V. Harok and K. Neufuss, Elastic and Inelastic Effects in Compression in Plasma-Sprayed Ceramic Coatings, *J. Therm. Spray Technol.*, 2001, **10**(1), p 126-132
6. O. Kesler, J. Matejicek, S. Sampath, S. Suresh, T. Gnaeupel-Herold, P.C. Brand, and H.J. Prask, Measurement of Residual Stress in Plasma-Sprayed Metallic, Ceramic and Composite Coatings, *Mater. Sci. Eng. A*, 1998, **257**(2), p 215-224
7. J. Matejicek and S. Sampath, In Situ Measurement of Residual Stresses and Elastic Moduli in Thermal Sprayed Coatings. Part 1: Apparatus and Analysis, *Acta Mater.*, 2003, **51**(3), p 863-872
8. J. Nohava and F. Kroupa, Nonlinear Stress-Strain Behavior of Plasma Sprayed Ceramic Coatings, *Acta Technica CSAV*, 2005, **50**(3), p 251-262
9. O. Kovarik, J. Siegl, J. Nohava, and P. Chraska, Young's Modulus and Fatigue Behavior of Plasma-Sprayed Alumina Coatings, *J. Therm. Spray Technol.*, 2003, **14**(2), p 231-238